

Gamma-ray observations of the microquasars Cygnus X-1, Cygnus X-3, GRS 1915+105, and GX 339–4 with the *Fermi* Large Area Telescope

Arash Bodaghee

Space Sciences Laboratory, 7 Gauss Way, University of California, Berkeley, CA 94720, USA
bodaghee@ssl.berkeley.edu

John A. Tomsick

Space Sciences Laboratory, 7 Gauss Way, University of California, Berkeley, CA 94720, USA

Katja Pottschmidt

CRESST and NASA Goddard Space Flight Center, Astrophysics Science Division, Code 661, Greenbelt, MD 20771, USA
Center for Space Science and Technology, University of Maryland Baltimore County, 1000 Hilltop Circle, Baltimore, MD 21250, USA

Jérôme Rodriguez

Laboratoire AIM, CEA/IRFU - Université Paris Diderot - CNRS/INSU,
CEA DSM/IRFU/SAP, Centre de Saclay, F-91191 Gif-sur-Yvette, France

Jörn Wilms

Dr. Karl Remeis-Sternwarte and Erlangen Centre for Astroparticle Physics, Friedrich-Alexander-Universität Erlangen-Nürnberg, Sternwartstraße 7, 96049 Bamberg, Germany

Guy G. Pooley

The University of Cambridge, Mullard Radio Astronomy Observatory, Cavendish Laboratory,
J.J. Thomson Avenue, Cambridge CB3 0HE, UK

ABSTRACT

Detecting gamma-rays from microquasars is a challenging but worthwhile endeavor for understanding particle acceleration, the jet mechanism, and for constraining leptonic/hadronic emission models. We present results from a likelihood analysis on timescales of 1 d and 10 d of ~ 4 years worth of gamma-ray observations (0.1–10 GeV) by *Fermi*-LAT of Cyg X-1, Cyg X-3, GRS 1915+105, and GX 339–4. Our analysis reproduced all but one of the previous gamma-ray outbursts of Cyg X-3 as reported with *Fermi* or *AGILE*, plus 5 new days on which Cyg X-3 is detected at a significance of $\sim 5\sigma$ that are not reported in the literature. In addition, Cyg X-3 is significantly detected on 10-d timescales outside of known gamma-ray flaring epochs which suggests that persistent gamma-ray emission from Cyg X-3 has been detected for the first time. For Cyg X-1 we find three low significance excesses (~ 3 – 4σ) on daily timescales that are contemporaneous with gamma-ray flares reported (also at low significance) by *AGILE*. Two other microquasars, GRS 1915+105 and GX 339–4, are not detected and we derive 3σ upper limits of 2.3×10^{-8} ph cm $^{-2}$ s $^{-1}$ and 1.6×10^{-8} ph cm $^{-2}$ s $^{-1}$, respectively, on the persistent flux in the 0.1–10 GeV range. These results enable us to define a list of the general conditions that are necessary for the detection of gamma-rays from microquasars.

1. Introduction

A microquasar (μ QSO) consists of a compact object (CO: a neutron star, NS, or a black hole, BH) that accretes matter from a normal stellar companion. The characteristic that distinguishes μ QSOs from other X-ray binaries (XRBs) is the presence of non-thermal synchrotron emission from relativistic jets launched near the CO (Mirabel & Rodríguez 1999). These radio jets are believed to be powered by black-hole spin and/or by strong electromagnetic currents in the inner accretion disk (e.g., Blandford & Znajek 1977; Meier 2001).

The presence of jets interacting with plasmas within strong electromagnetic and gravitational fields leads μ QSOs to display rapid variability across a broad range of frequencies: from radio, to IR, and X-rays. A few of these objects have been detected in the gamma-rays (>100 MeV) with *AGILE* (Tavani et al. 2009b), *Fermi*-LAT (Atwood et al. 2009), and *MAGIC* (Lorenz 2004, and references therein). These are Cyg X-3 (Abdo et al. 2009c; Tavani et al. 2009a; Corbel et al. 2012; Piano et al. 2012) and Cyg X-1 (Albert et al. 2007; Bulgarelli et al. 2010a; Sabatini et al. 2010b,a, 2013). While the XRBs LS I+61°303 (Albert et al. 2006; Abdo et al. 2009a) and LS 5039 (Paredes et al. 2000; Aharonian et al. 2005; Abdo et al. 2009b) have been detected at MeV–TeV energies, it is still uncertain whether they should be classified as μ QSOs (e.g., Paredes 2011a).

Leptonic and hadronic processes are generally invoked to explain gamma-ray emission from μ QSOs. In the former, relativistic electrons in the jet emit synchrotron radiation (with some loss due to self-absorption), or they can Compton upscatter low-energy (IR and UV) photons from the accretion disk or from the stellar companion to gamma-ray energies (e.g., Kaufman Bernadó et al. 2002; Romero et al. 2002; Bosch-Ramon et al. 2006; Sitarek & Bednarek 2012, and references therein). In hadronic models, inelastic collisions between jet protons and those of the dense stellar wind produce neutral pions which decay into gamma-rays and neutrinos (e.g., Romero et al. 2003, and references therein). Interactions between the jet and the clumpy winds from massive donor stars in HMXB microquasars can lead to gamma-ray emission from both leptonic (IC) and hadronic (neutral pion decay) processes (Araudo et al. 2009; Owocki et al. 2009). These winds can also serve as the site for the initiation of e^-e^+ cascades from a primary source

of very-high energy (VHE) gamma-rays within the system; the secondary emission resulting from these pair cascades should be detectable in the low-energy gamma-rays (Bednarek 1997; Romero et al. 2010). Some of these photons can be absorbed by the wind leading to variable gamma-ray emission (Dubus 2006). Shocks at the termination zone where the jet meets the interstellar medium are also believed to produce gamma-ray photons (Bosch-Ramon et al. 2011).

The common trait shared by these emission models is that gamma-rays are tied to the presence of radio jets (Paredes 2011b). These jets appear during specific emission states for black-hole XRBs (BHXBs: e.g., Fender et al. 2004; McClintock & Remillard 2006, and references therein). Indeed, this link between radio and gamma-ray emission was demonstrated for several gamma-ray outbursts of Cyg X-3 (Corbel & Hays 2010; Williams et al. 2011; Corbel et al. 2012). It is clear then that observations of this class of objects in the gamma-rays can shape our understanding of the role jets play in particle acceleration and the production of high-energy photons.

In this paper, we present a systematic study of four well-known μ QSOs (Cyg X-1, Cyg X-3, GRS 1915+105, and GX 339–4) using gamma-ray data collected by the Large Area Telescope on board the *Fermi* space telescope. In § 2, the sources selected for this study are introduced, and the dataset and analysis techniques are described. We present results for individual objects in § 3, and we discuss their implications in § 4. A summary of our key findings is given in § 5.

2. Source List & Data Analysis

2.1. Source List

Our source list consists of the four μ QSOs presented in Table 1. All four systems happen to host black hole candidates even though μ QSOs can sometimes host neutron stars (Fender 2002, and references therein). In recent years, these μ QSOs have displayed a wide range of X-ray luminosities and state changes, and so they are the regular subjects of observations by telescopes in all wavelengths. Of these sources, only Cygnus X-3 was unambiguously detected in the gamma-rays (with *AGILE* and *Fermi*). There are reports of possible gamma-ray emission from Cyg X-1 detected by *AGILE* (Bulgarelli et al. 2010a; Sabatini et al. 2010b,a, 2013) but the detection significances are low ($\sim 3\text{--}4\sigma$) and these have not yet been corroborated with *Fermi* detections. The pri-

TABLE 1
MICROQUASAR CANDIDATES SELECTED FOR THIS STUDY.

Name	R.A. (J2000) [deg]	Decl. (J2000) [deg]	P_{orb} [d]	Distance [kpc]	Type [†]
Cygnus X-1	299.590	+35.202	5.599829(16) ^a	1.86 ^{+0.12} _{-0.11} ^b	HMXB
Cygnus X-3	308.107	+40.958	0.1996907(7) ^c	7.2(5) ^d	HMXB
GRS 1915+105	288.798	+10.946	33.5(1.5) ^e	11 ⁺¹ ₋₄ ^f	LMXB
GX 339-4	255.706	-48.790	1.7563(3) ^g	10 ⁺⁵ ₋₄ ^g	LMXB

[†]HMXB: high-mass X-ray binary; LMXB: low-mass X-ray binary

References. — (a) Brocksopp et al. (1999); (b) Reid et al. (2011); (c) Wen et al. (2006); (d) Ling et al. (2009); (e) Harlaftis & Greiner (2004); (f) Jonker & Nelemans (2004); (g) Hynes et al. (2004).

mary objectives of this work are to reproduce previous gamma-ray detections of Cyg X-3 with the *Fermi*-LAT, and to apply a systematic search for possible gamma-ray emission from other μ QSOs. A brief description of these μ QSOs is provided in the following paragraphs.

2.1.1. Cygnus X-3

Discovered in the X-rays by Giacconi et al. (1967), Cyg X-3 was subsequently detected in the radio band (Braes & Miley 1972), and has since been observed and extensively studied in all wavelengths, including in the gamma-rays (Abdo et al. 2009c; Tavani et al. 2009a; Williams et al. 2011, e.g.). The compact object in Cyg X-3 is believed to be a black hole (e.g. Shrader et al. 2010; Zdziarski et al. 2013) in a tight orbit around a Wolf-Rayet star (van Kerkwijk et al. 1992). This configuration (a relativistic jet near a dense stellar wind) leads to gamma-ray emission that is modulated with the 4.8 h orbital period (Abdo et al. 2009c; Dubus et al. 2010).

Around a dozen outbursts from this source have been detected above 100 MeV by *Fermi* (Corbel et al. 2012) and *AGILE* (Piano et al. 2012). Multi-wavelength analysis of these gamma-ray outbursts led Corbel et al. (2012) to propose a set of three conditions that appear to be necessary for the detection of gamma-rays with the LAT: the source count rate in the *RXTE*-ASM 3–5 keV band should be higher than about 3 cts s⁻¹; the count rate in the *Swift*-BAT 15–50 keV band must cross (in either direction) the critical value of 0.02 cts s⁻¹; and there should be significant emis-

sion in the radio (flux densities $\gtrsim 0.2$ – 0.4 Jy). Whenever gamma-rays from this source are detected by the LAT, it is contemporaneous, but not necessarily coincident, with these conditions being satisfied. The order in which these various components (radio, X-rays, and gamma-rays) are emitted is not well understood with a time lag of $\Delta t = 5 \pm 7$ d between the peak emission in the radio band and in the gamma-rays (Abdo et al. 2009c).

2.1.2. Cygnus X-1

Located at a parallax-derived distance of 1.86^{+0.12}_{-0.11} kpc (Reid et al. 2011), Cyg X-1 (Bowyer et al. 1965) is a bright, nearby μ QSO featuring a likely black hole accreting from a high-mass companion with a binary orbital period of 5.6 d (e.g., Gies et al. 2008). Cyg X-1 is a persistent X-ray emitter: its X-ray evolution does not follow a q-shaped track in the hardness-intensity diagram as is typically seen in transient systems (e.g., Fender et al. 2004; Wilms et al. 2006). Instead, the source shows very fast (or sometimes failed) state transitions (e.g., Böck et al. 2011; Grinberg et al. 2013). This object is one of the best-studied X-ray sources in the Galaxy with firm detections from the radio band to the X-rays, and in the soft gamma-rays ($\lesssim 10$ MeV) with *COMPTEL* (McConnell et al. 2002) and with *AGILE* (>30 MeV: Bulgarelli et al. 2010a; Sabatini et al. 2010b,a, 2013). Polarized gamma-ray emission up to 2 MeV, whose likely origin is the jet, was detected with *INTEGRAL* (Laurent et al. 2011). At even higher energies (>100 GeV), a brief 4σ excess was reported with *MAGIC* (Albert et al. 2007) coinci-

dent with the beginning of a long-term brightening in the X-rays.

2.1.3. *GRS 1915+105*

An accreting black hole candidate in an LMXB system with a 33-d orbital period (e.g., Harlaftis & Greiner 2004), *GRS 1915+105* has been in outburst since 1992 when it was discovered in the hard X-rays by *Granat* (Castro-Tirado et al. 1992). Apparent superluminal motion in the ejecta of its radio jets is one remarkable feature of this object (Mirabel & Rodríguez 1994). Another interesting feature is its wide range of X-ray variability classes (e.g., Belloni et al. 2000; Klein-Wolt et al. 2002; Hannikainen et al. 2005). Thus, *GRS 1915+105* is one of the brightest and most variable sources in the X-ray sky making it a prime target for multi-wavelength campaigns from the radio to the hard X-ray band seeking to understand accretion physics around black holes and the interactions between the accretion disk and the relativistic jets (Rodríguez et al. 2008a,b). Non-thermal emission (i.e., from the jets or at the termination shock) could extend up to very high-energy (VHE) gamma-rays, however, such emission has not been detected from this source with, e.g., *HESS* (Szostek et al. 2009), nor has it been detected in soft gamma-rays with *Fermi* or *AGILE*.

2.1.4. *GX 339–4*

A recurrent X-ray transient, *GX 339–4* (Markert et al. 1973) is composed of a black hole candidate in a 1.8-d orbit (Jonker & Nelemans 2004) around a low-mass donor star (Hynes et al. 2003, 2004). The source undergoes regular outbursts in the X-rays which trace a q -track in the hardness-intensity diagram (Belloni et al. 2005). This system features powerful relativistic jets that are suppressed in the high-soft state (Corbel et al. 2000) leading to the discovery of a strong correlation between radio and hard X-ray emission (Fender et al. 1999; Corbel et al. 2003). The distance to *GX 339–4* is not well known (see discussion in, e.g., Zdziarski et al. 2004) but is suspected of being between 6 kpc and 15 kpc (Hynes et al. 2004; Zdziarski et al. 2004). Gamma-ray emission is expected from this μ QSO (e.g., see discussion in Vila & Romero 2010) but efforts to detect this emission have been unsuccessful.

2.2. Data Analysis

Fermi Science Tools v9r27 and HEASoft 6.12 were used to analyze all photon events within 20° of the sources listed in Table 1 that were captured by the *Fermi* Large Area Telescope (LAT: Atwood et al. 2009) between the first full day of data availability (2008 August 5: MJD 54683) and 2012 May 15 (MJD 56062). Good time intervals were selected for two energy bands (100 MeV–1 GeV and 100 MeV–10 GeV) with `gtselect` and `gtmktime`. The events class was set to “2” which selects only high-quality diffuse photons. To minimize background albedo photons from the Earth’s limb, we restricted the zenith and rocking angles to less than 100° and 52° , respectively. The scripts `gtexpcube` and `gtexmpap` generated exposure maps while `gtbin` created photon counts maps in the region of interest. The instrument response functions consisted of `P7SOURCE_V6`.

To create light curves on short timescales, the spatial distribution of known sources and their spectral parameters must be modeled as accurately as possible. Counts maps created from the full data set are presented in Fig. 1. Visual inspection of these fields reveals the challenge in assigning photons to our targeted sources.

The BHXB state with the highest X-ray luminosity is usually the steep-power-law state (McClintock & Remillard 2006) which features a photon index $\Gamma > 2.4$, and a variable hard tail that can extend to ~ 1 MeV (McClintock & Remillard 2006). While the X-rays and gamma-rays could have different power-law slopes (Corbel et al. 2012), we note that a photon index $\Gamma = 2.7$ was measured with *Fermi*-LAT during gamma-ray outbursts of Cyg X-3 (Abdo et al. 2009c). This suggests that our targets should be faint, and any emitted gamma-rays are more likely to be found at the low end of the *Fermi* energy band ($\lesssim 1$ GeV). At these energies, the LAT point spread function (PSF) is of the order of a degree or more. Photons emanating from our targets (and from other sources) are spread across the images (and partially beyond). Our targets are situated near the Galactic Plane where there is a high level of diffuse background emission whose intensity peaks in the energy range of interest. Their spatial and spectral distributions are not well understood but they must be accounted for, nonetheless.

For each target, we began with a model file that included all 2FGL sources (The *Fermi*-LAT Collaboration 2011) located up to 5° away from the target po-

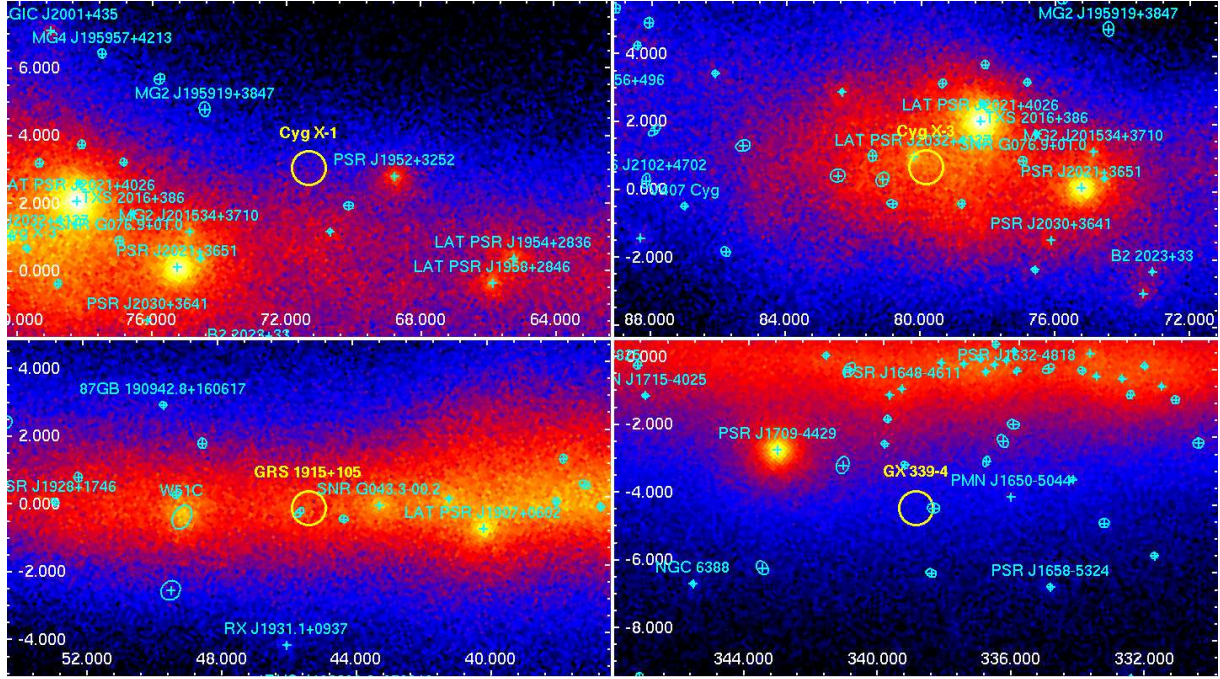


Fig. 1.— Photon counts map (in Galactic coordinates) of an $18^\circ \times 10^\circ$ field around the microquasars in our study from LAT data (0.1–10 GeV) spanning 2008 August 5 through 2012 May 15. Galactic coordinates are shown as are the locations of sources from the 2FGL catalog (The Fermi-LAT Collaboration 2011) that are included in the likelihood analysis; the symbol size represents the 95-% error ellipse. The position of each microquasar is indicated by a 1° -diameter circle.

sition, and all bright (detection significance $> 7\sigma$ and flux ($>100\text{ MeV}$) $> 5 \times 10^{-8} \text{ ph cm}^{-2} \text{ s}^{-1}$) 2FGL sources up to 20° away. We also included the latest spectral and spatial models for the Galactic (`gal_2yearp7v6_v0`) and extragalactic (`iso_p7v6source`) diffuse emission. A binned likelihood analysis (`gtlike`) was performed on the full data set (0.1–1 GeV and 0.1–10 GeV) where sources within 3° of the target (including the diffuse emission components) had spectral parameters that were allowed to vary, while sources within 9° of our target had free normalizations. This enabled the spectral parameters of sources in the field to be constrained. A new model file was made in which all spectral parameters were fixed to the values derived from this binned analysis, except for the photon index and normalization of the target μQSO which were left free to vary.

Then, we performed an unbinned likelihood analysis in the 0.1–1 and 0.1–10 GeV energy range in three time bins: 0.1, 1, and 10 days. Only photons inside

a circle of 7° radius centered on the target were considered in the likelihood analysis. Restricting the energy range to lower values (0.1–1 GeV) increases the probability that the gamma-ray photons originate from our target, since these sources are expected to emit few photons above 1 GeV. However, any gain in likelihood is offset by a higher background due to the larger size of the LAT PSF at low energies. There are no significant differences in the light curves generated from the likelihood analysis in the 0.1–1 GeV and 0.1–10 GeV range (other than the aforementioned higher level of background in the former), so only the 0.1–10 GeV results are discussed hereafter. We note that in the current version of the *Fermi* Science Tools, an unbinned likelihood analysis of a faint source in the Galactic Plane can lead to an overestimation of the test statistic (TS^1). However, this effect should have a minimal impact on our analyses since the bias increases with exposure time whereas we are concentrating on exposures between 0.1–10 d.

¹http://fermi.gsfc.nasa.gov/ssc/data/analysis/LAT_caveats.html

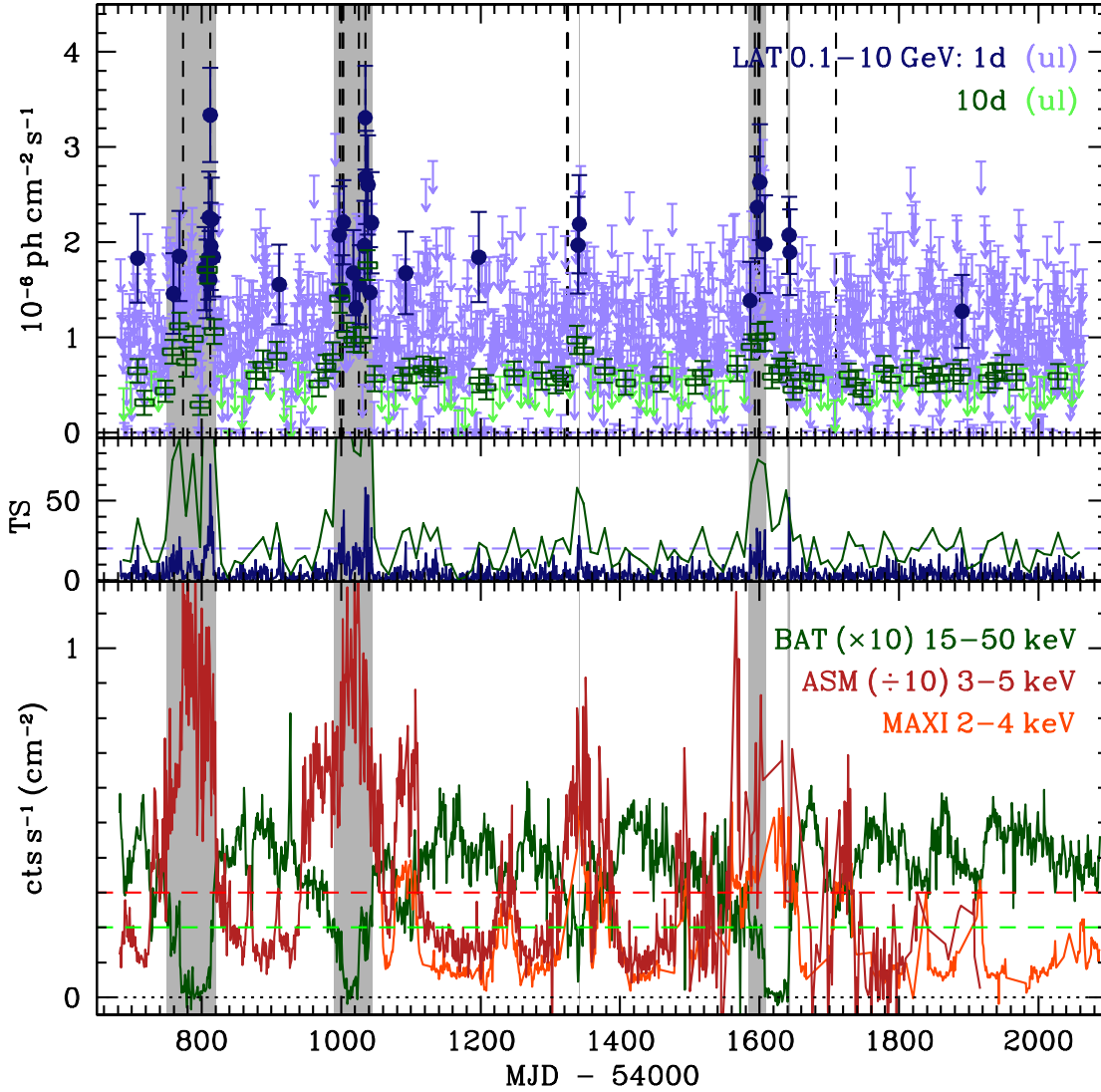


Fig. 2.— Light curve of Cyg X-3 as collected from a likelihood analysis of *Fermi*-LAT (0.1–10 GeV) data taken between 2008 August 5 and 2012 May 15. Results are presented for 1-day and 10-day bins where the top panel presents the integrated flux (in 10^{-6} ph cm^{-2} s^{-1}) while the middle panel gives the corresponding test statistic (TS). Bins in which $\text{TS} \geq 20$ (horizontal dashed line in the middle panel) are represented by disks (1-day) and rectangles (10-day) in the top panel, while downward arrows represent $1-\sigma$ upper limits for bins with $\text{TS} < 20$. Previously-reported gamma-ray detections by *AGILE* (vertical dashed lines in the top panel) and by *Fermi*-LAT (shaded regions) are also shown. The bottom panel presents the daily light curves in soft and hard X-rays from *MAXI*-GSC (cts s^{-1} cm^{-2} in 2–4 keV), *RXTE*-ASM (cts s^{-1} in 3–5 keV), and *Swift*-BAT (cts s^{-1} cm^{-2} in 15–50 keV). In this panel, the horizontal dashed lines denote the X-ray thresholds defined by Corbel et al. (2012) for its detection in gamma-rays, i.e., an ASM count rate ≥ 3 cts s^{-1} , and a BAT count rate crossing 0.02 cts s^{-1} , respectively. Error bars have been omitted for clarity.

3. Results

3.1. Cygnus X-3

Figure 2 presents the light curve for Cyg X-3 resulting from the unbinned LAT likelihood analysis, i.e., the source photon flux integrated over the 0.1–10 GeV energy range, its error, and a test statistic ($TS \sim -2 \ln L$ where L is the ratio of the likelihood of models with and without the source of interest, c.f., Mattox et al. 1996). Test statistics and their corresponding significances ($\sigma \sim \sqrt{TS}$) are not trial-corrected. For time bins in which $TS < 20$, a $1\text{-}\sigma$ upper limit on the flux is plotted instead.

Provided for comparison are the daily light curves in soft and hard X-ray bands from *MAXI*-GSC (2–4 keV), *RXTE*-ASM (3–5 keV), and *Swift*-BAT (15–50 keV)². Note the significant degradation of the ASM data towards the end of the *RXTE* mission lifetime (after MJD 55200: e.g., Grinberg et al. 2013). As can be seen in Fig. 2, the gamma-ray sampling by the LAT covers a wide range of spectral states (and transitions). Table 2 summarizes the daily gamma-ray detections of Cyg X-3 and the corresponding X-ray count rates. References to gamma-ray detections reported within 3 days of these dates are included.

Our analysis of Cyg X-3 reproduced all previously-reported gamma-ray outbursts detected with LAT (Abdo et al. 2009c; Corbel & Hays 2010; Williams et al. 2011; Corbel et al. 2011, 2012) at comparable fluxes and TS values ($F_{\geq 100\text{MeV}} = (1-4) \times 10^{-6} \text{ ph cm}^{-2} \text{ s}^{-1}$). The source has also been detected on several occasions with *AGILE* (Bulgarelli et al. 2010b, 2011b,c,a; Piano et al. 2011, 2012), and these are indicated in Fig. 2 by ticks at the top of each panel. We can confirm significant LAT detections ($TS \geq 20$) around these dates for all but one of these: 2011 May 28 (MJD 55709: Piano et al. 2011) which happens to be the last reported gamma-ray outburst from this source.

There are 5 new days not previously reported with either *Fermi* or with *AGILE* during which the flux from Cyg X-3 is detected at a significant level by the LAT: these are MJD 54708, 54911, 55092, 55197, and 55890 (Table 2). The light curve binned at 10 d also shows significant gamma-ray emission ($TS \geq 20$) for bins that overlap these new daily outbursts.

Another way to visualize the X-ray and gamma-ray

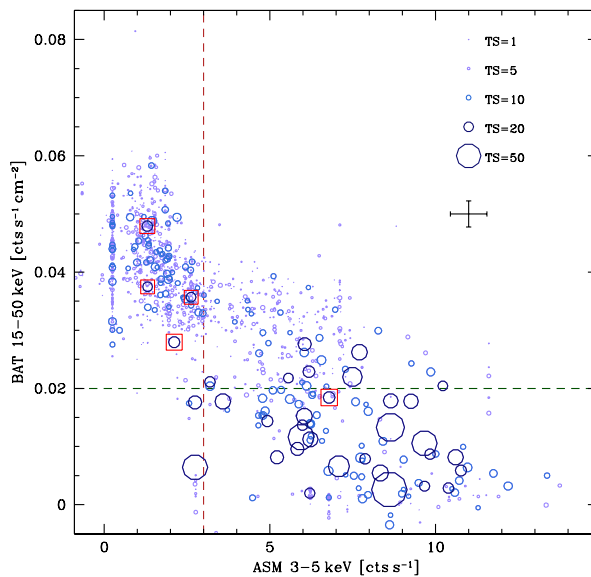


Fig. 3.— Distribution of daily TS values (0.1–10 GeV) for Cyg X-3 in the ASM vs. BAT count-rate plane. The radius of each circle is proportional to the TS measured on that day, and it is centered on the reported ASM (3–5 keV) and BAT (15–50 keV) count rates for that day when they are available (or on the nearest date). The average 1σ uncertainty in both directions is shown as a cross. Days with $TS \geq 20$ are plotted with dark symbols, while the 5 new daily detections are boxed. The vertical dashed line indicates a count rate of 3 cts s^{-1} in the ASM band while the horizontal dashed line denotes a count rate of 0.02 cts s^{-1} in the BAT band.

data is shown in Fig. 3 where the distribution of daily TS values obtained for Cyg X-3 is plotted in the ASM vs. BAT count-rate plane. Each circle in this plot is proportional in size to the daily TS value obtained for Cyg X-3 and is centered at the reported ASM and BAT count rates on that day. In cases where either ASM or BAT did not provide a daily count rate, we used the values from the nearest date so as to not discard information. Occasionally, this leads to vertical streaks in the distribution. For example, days from the last ~6 months of LAT data used in this analysis were gathered when *RXTE* was no longer operating so they share the last reported ASM count rate of 0.245 cts s^{-1} . The average error on the count rate in both X-ray bands is denoted by a cross.

Visible is the expected hard (BAT) to soft (ASM)

²<http://maxi.riken.jp>
http://xte.mit.edu/ASM_lc.html
<http://heasarc.gsfc.nasa.gov/docs/swift/results/transients>

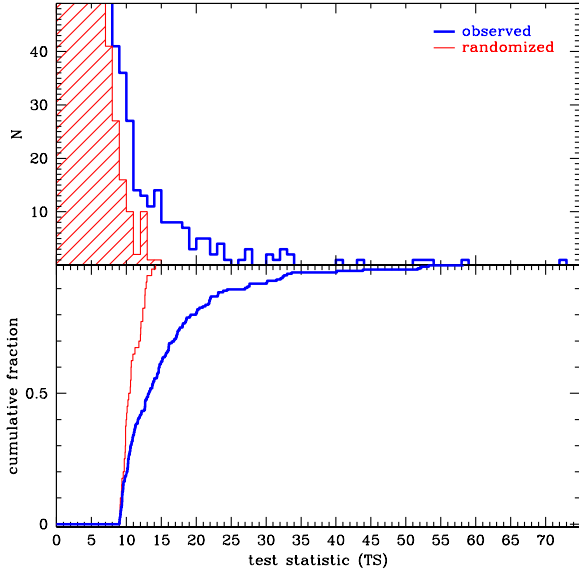


Fig. 4.— Distributions of the test statistic (TS) from an unbinned likelihood analysis of daily LAT data of Cyg X-3 (observed), compared with those from a spurious unidentified gamma-ray source that follows a randomized χ^2_3 distribution (randomized). Restricting the cumulative distributions to $TS \geq 9$ and applying a KS-test yields a low probability ($< 10^{-10}$) of statistical compatibility.

X-ray anti-correlation despite the large scatter in the data. Days for which Cyg X-3 presented a high TS value (large circles) tend to be located in the lower right portion of the plot; in the parameter space defined by Corbel et al. (2012) that appear necessary for gamma-ray emission from Cyg X-3. This is when Cyg X-3 emits over 3 cts s^{-1} in the ASM band (3–5 keV), and crosses the critical value of 0.02 cts s^{-1} in the BAT band (15–50 keV). A multiplicative factor of ~ 0.05 is required to convert count rates from ASM to *MAXI* (2–4 keV).

These X-ray conditions from Corbel et al. (2012) were met or close to being satisfied on almost all days for which $TS \geq 20$, possibly meeting them on timescales less than the 1-d binning used in the light curve. On the other hand, the X-ray conditions are often satisfied without a corresponding daily LAT detection; this is evident in the large number of low-TS value circles located within this region.

In Fig. 4, we present the distribution of daily TS

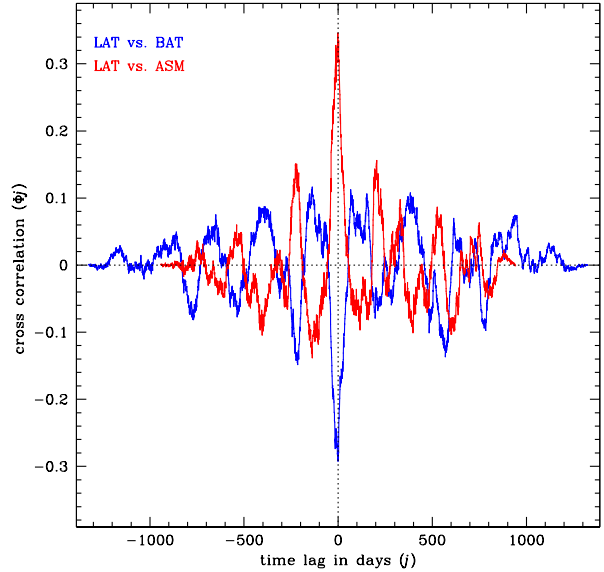


Fig. 5.— Discrete cross-correlation functions for Cyg X-3 comparing daily LAT (0.1–10 GeV) light curve data with those from ASM (3–5 keV: solid curve) and BAT (15–50 keV: dashed curve).

values from Cyg X-3 as compared with a distribution of TS values that follows a randomized χ^2_3 distribution (i.e., the expected TS distribution for a spurious unidentified gamma-ray source: Mattox et al. 1996). We are mainly interested in TS values of 9 or above, and the distributions diverge below this value, so we drew the cumulative distributions of the samples for $TS \geq 9$ and applied the Kolmogorov-Smirnov (KS) test. We obtain a very low KS-test probability (less than 10^{-10}) of statistical compatibility between the observed and randomly-generated distributions.

Figure 5 shows the discrete cross-correlation function of Cyg X-3 comparing the light curve in gamma-rays with those from soft (ASM) and hard (BAT) X-rays. Deviations from cross-correlation $\phi_j = 0$ are $\lesssim 35\%$ and are likely the result of instrumental effects such as the 57-d precession period of the *Fermi* space telescope (and other known *Fermi* periods such as at 96 min, 3.2 hr, 1 d and 91 d: R.H.D. Corbet, private communication).

It has been proposed by Abdo et al. (2009c) that gamma-ray emission from Cyg X-3 is maximized at superior conjunction, i.e., when the compact object and its jet are irradiated by the WR star with respect

to our line of sight. We checked whether the 5 new daily detections of Cyg X-3 occurred at specific binary orbital phases by using the updated ephemerides of Zdziarski et al. (2012) to assign the orbital phase to the events file. Merging the events files from the 5 new daily detections into a single file enables us to visually confirm the 96 min and 3.2 hr periodicities which are due to the orbital period of the *Fermi* spacecraft. Because these periodicities are strong compared to the emission from Cyg X-3, we are unable to measure a significant increase in events coincident with certain phases of the expected 4.8-hr binary orbital period. This is true even when we focus on the day during which the TS is highest (MJD 54812). The binary period is also absent from the 0.1-d light curve generated from a likelihood analysis of the full data set which yields a significant detection only at the 57-d *Fermi* precession period. On the other hand, orbital modulations in the gamma-rays have only been detected during gamma-ray flaring epochs (Corbel et al. 2012), and the likelihood analysis is not recommended for exposures shorter than ~ 1 day, so other methods such as aperture-restricted event-weighting and epoch-specific analyses (e.g., as in Corbet et al. 2011; Corbel et al. 2012) are more appropriate.

Figure 2 showed good overall consistency between the 1-d and 10-d LAT light curves. In addition, the 10-d binned light curve reveals numerous significant detections ($TS \geq 20$) of Cyg X-3 both in and out of the expected gamma-ray active states. This could be the signature of faint, persistent gamma-ray emission from Cyg X-3, but another possibility is that these are contaminating photons originating from PSR J2032+4127 which is located around $30'$ away. Unlike in previous studies (Abdo et al. 2009c; Williams et al. 2011; Corbel et al. 2012), in our likelihood analysis of Cyg X-3, events corresponding to the on-pulse phases of this nearby pulsar were not removed.

To test the degree to which PSR J2032+4127 contributes to the gamma-ray flux at the location of Cyg X-3, we restricted the event times to an interval in which gamma-ray photons from Cyg X-3 have been confirmed by the LAT and by *AGILE*: between MJD 54990 and MJD 55045. Phase information from the latest gamma-ray ephemeris of PSR J2032+4127 from Ray et al. (2011) was added to the events file of this time interval, and a new events file was generated in which the on-pulse phases were excluded. These are phases $0.0 \leq \Phi \leq 0.15$, $0.5 \leq \Phi \leq 0.6$, and

$0.95 \leq \Phi \leq 1.0$ (c.f., Fig. 52 of Ray et al. (2011)). This removed 30% of the live-time and so the exposure time of the resulting events file was adjusted accordingly. We ran the likelihood analysis considering the full 55-d interval as a single observation. In this case, the spectral parameters of sources located within 3° of Cyg X-3 (including PSR J2032+4127 and the diffuse emission components) were allowed to vary, while normalizations were variable for sources out to a larger radius (9°) around Cyg X-3.

Discarding the on-pulse times removed nearly all photons from PSR J2032+4127, and it leads to a 30% reduction in the photon counts from Cyg X-3 and a similar reduction in the sum total of the photon counts from all sources in the field. This is consistent with the number of photons that would have been counted in the amount of exposure time that was removed. In conclusion, PSR J2032+4127 is not contributing significant numbers of unaccounted-for photons at the position of Cyg X-3 which makes it unlikely to be the source of persistent emission.

We can not completely rule out contaminating emission from other sources in the field, including the diffuse galactic and extragalactic background, as the source of the faint, persistent emission detected at the location of Cyg X-3. However, the bulk of the emission from other field sources is accounted for in the spectral models provided by the LAT team, and especially in the refined spectral models that we generated from the binned analysis of the long-term dataset. As we show in the next section, this underlying emission is not present in the 10-d binned light curve of Cyg X-1 which is also located in this field. This suggests that the 10-d detections in and out of previously-reported gamma-active epochs are likely to be from Cyg X-3 which means that persistent gamma-ray emission is being detected from a μ QSO for the first time.

3.2. Cygnus X-1

In the 1369 days of gamma-ray monitoring by the LAT (Fig. 6), the TS value reached a level of 9 ($\sim 3\sigma$) or above on the 21 days listed in Table 3. Three of these candidate gamma-ray detections of Cyg X-1 by the LAT are contemporaneous with possible gamma-ray detections reported in the literature by *AGILE*. In all three cases, the possible 1-d detections by LAT precede the detections reported with *AGILE* by 1–2 days.

On 2009 October 14 (MJD 55118), we obtained a candidate detection of Cyg X-1 with the LAT at a TS

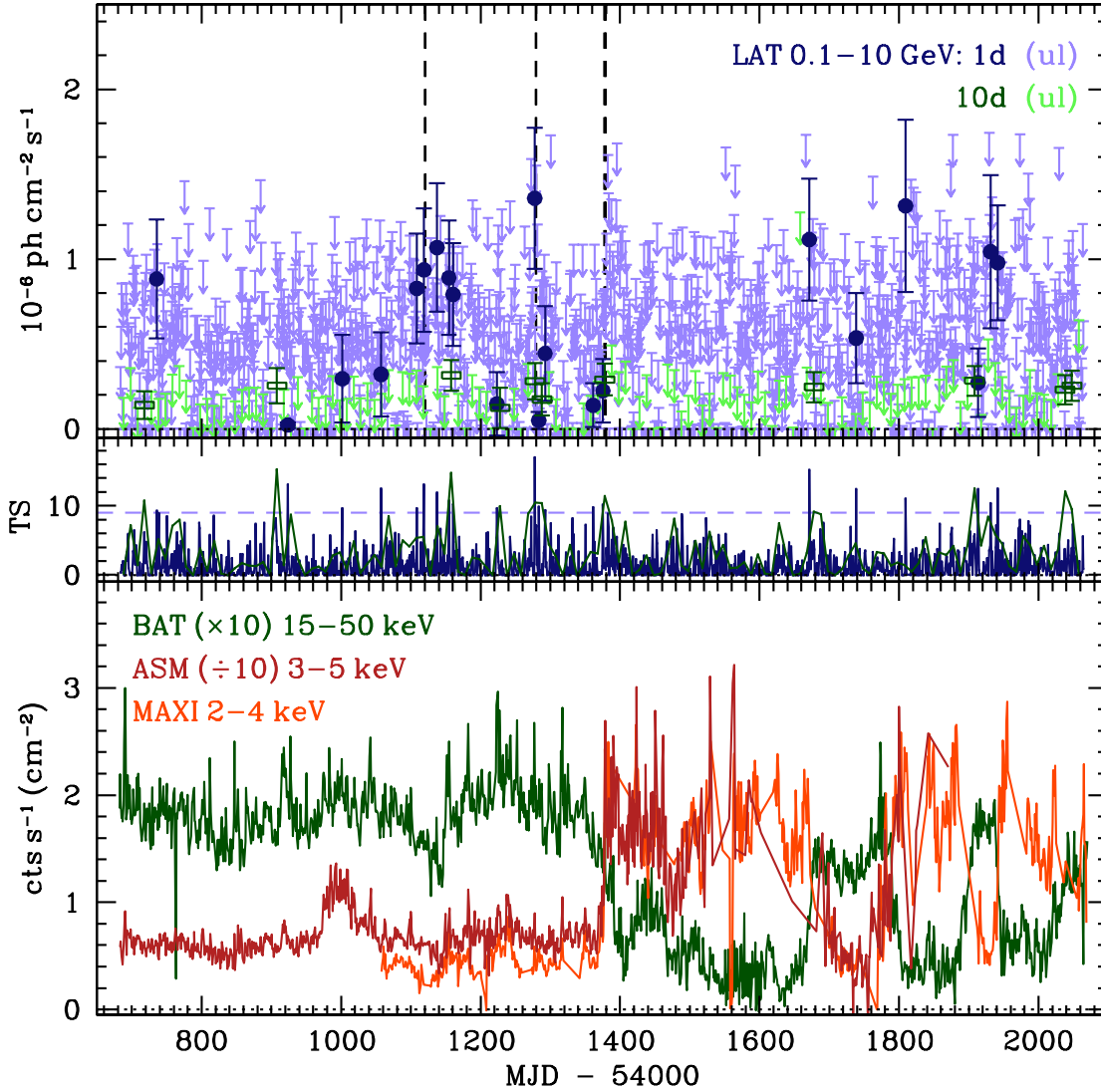


Fig. 6.— Same as Fig. 2 for Cyg X-1 with a TS threshold of 9 (horizontal dashed line in the middle panel).

value of 13 ($\sim 3.6\sigma$). This was only 1–2 days before Sabatini et al. (2010b) reported a short (1-d long) outburst at the location of Cyg X-1 with *AGILE* (see also Sabatini et al. 2013). With the LAT, we measured a source flux of $(1.1 \pm 0.4) \times 10^{-6} \text{ ph cm}^{-2} \text{ s}^{-1}$ in 0.1–10 GeV, i.e., slightly lower than, but statistically compatible with, the flux reported with *AGILE*.

The maximum value of $\text{TS}=17$ ($\sim 4\sigma$) was reached on 2010 March 22 (MJD 55277), i.e., 1–2 days

before a gamma-ray flare was detected by *AGILE* (Bulgarelli et al. 2010a). On this date, LAT recorded a source flux of $(1.4 \pm 0.4) \times 10^{-6} \text{ ph cm}^{-2} \text{ s}^{-1}$ (0.1–10 GeV), i.e., consistent with the flux reported by *AGILE* in a similar band: $(2.0 \pm 0.9) \times 10^{-6} \text{ ph cm}^{-2} \text{ s}^{-1}$. Figure 7 presents a spatial map of the TS value on MJD 55277 generated by modeling all sources except for Cyg X-1. A bright cluster of pixels can be seen consistent with the location of Cyg X-1. The large

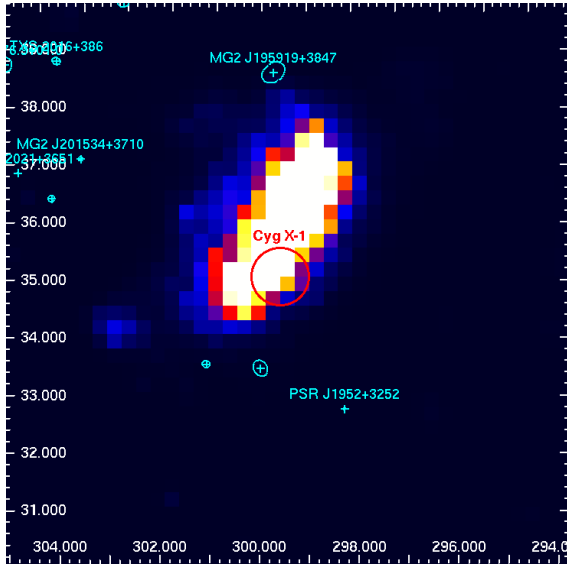


Fig. 7.— Differential test statistic (TS) map of a $10^\circ \times 10^\circ$ field centered on Cyg X-1 from LAT data (0.1–10 GeV) during MJD 55277. Each pixel is 0.25° wide, and in the lightest regions, the TS values range from 15 to 17 ($\sim 4\sigma$).

size of this pixel cluster and its offset with respect to Cyg X-1, both of which are also seen in *AGILE* TS maps of this source (Sabatini et al. 2013), can be explained by the $\sim 2^\circ$ -diameter of the PSF at these energies and the low photon counts.

Around the time of the third *AGILE* detection (beginning on 2010 June 30 or MJD 55377; Sabatini et al. 2010a, 2013), we obtained with LAT on 2010 June 28 (MJD 55375) a TS value of 10 ($\sim 3\sigma$) at a flux of 2×10^{-7} $\text{ph cm}^{-2} \text{s}^{-1}$, i.e., less than the flux of 10^{-6} $\text{ph cm}^{-2} \text{s}^{-1}$ measured with *AGILE*. Figure 6 shows that this date corresponds to an epoch in which Cyg X-1 was undergoing a hard-to-soft state transition (Negoro et al. 2010; Rushton et al. 2010; Wilson-Hodge & Case 2010). There are no reports of contemporaneous radio flaring which is sometimes seen during such transitions (e.g. Cadolle Bel et al. 2006; Wilms et al. 2007). Monitoring around this time shows that the radio emission was briefly quenched (MJD 55386: Rushton et al. 2012) and then showed the possible spectral signatures of discrete ejection events (MJD 55400: Tudose et al. 2010).

Given that there are contemporaneous (but not coincident) detections with *AGILE* for MJD 55118, MJD 55277, and MJD 55375, it is not necessary to

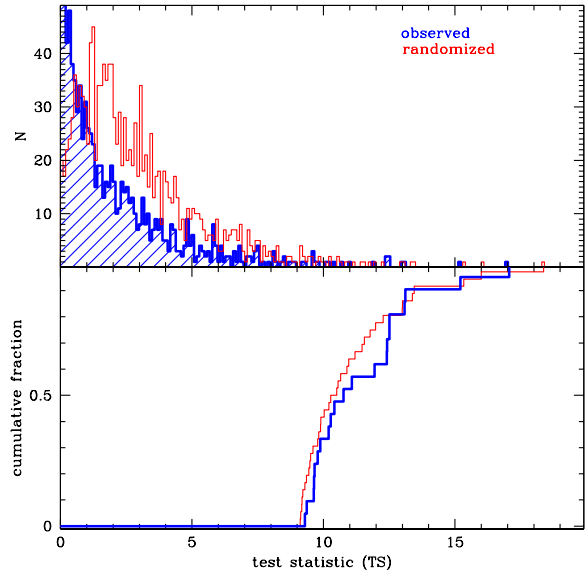


Fig. 8.— Same as Fig. 4 for Cyg X-1. For $\text{TS} \geq 9$, the probability of statistical compatibility from a KS-test is 55%.

apply a trial correction to the detection significances that we obtained on these dates. For the other days listed in Table 3, the requirement to correct for the number of blind-search trials can be relaxed if it can be shown that these dates correspond to likely gamma-ray emission states from Cyg X-1, e.g., states in which the jet is present. The intermediate state of Cyg X-1 is thought to feature the formation and destruction of relativistic jets, while compact jets (lower bulk velocity, and hence, less energetic than the relativistic jets) are believed to always be present during the hard state (Stirling et al. 2001; Fender et al. 2009).

We identified the most likely state of Cyg X-1 by employing the prescription of Grinberg et al. (2013) based on *RXTE* and *MAXI* count rates. There are 5 days listed in Table 3 in which Cyg X-1 was in the transitional/intermediate state (MJD 55001, 55160, 55671, 55913, and 55941), and 1 day (MJD 55809) where the source was in the soft state, which suggests that it passed through the intermediate state on timescales shorter than the binning that was used. The other dates in Table 3 had Cyg X-1 in the hard state.

As was done for Cyg X-3, we compared the observed TS distribution from Cyg X-1 with that of a randomly-generated light curve of a spurious uniden-

tified EGRET source (Fig. 8). For $TS \geq 9$, the KS-test probability of statistical compatibility is 55%. This suggests that low-significance LAT detections that are not contemporaneous with those of another gamma-ray instrument (e.g., *AGILE*), or for which there is no other compelling evidence that gamma-rays should be present, are likely spurious. Signatures of the 5.6-d binary orbital period of Cyg X-1 (e.g., Wen et al. 2006) could not be found in the 0.1-d light curve.

3.3. GRS 1915+105

The light curve of GRS 1915+105 from the likelihood analysis of 1-d and 10-d bins contains four days (out of 1371) on which the TS was above 9 (a maximum of 14.4 was reached on MJD 55110) with no 10-d bins having $TS \geq 9$ (Fig. 9 and Table 4). Comparing the observed daily TS distribution with that of a randomized TS distribution yields a KS-test probability of 83% of statistical compatibility between the distributions for $TS \geq 9$ (Fig. 10). This indicates that the low-significance detections are likely spurious. It is also clear that the source is not detectable on longer timescales of 1–2 years based on its absence from the 1FGL and 2FGL catalogs. We obtain a 3σ upper limit of $2.3 \times 10^{-8} \text{ ph cm}^{-2} \text{ s}^{-1}$ on the persistent flux from GRS 1915+105 in the 0.1–10 GeV range. This value was determined by considering the full 4-year data set as a single observation, and running the likelihood analysis where the spectral parameters of sources within 3° of GRS 1915+105 (including those of GRS 1915+105 and of the diffuse galactic and extragalactic components) were allowed to vary, while sources within 9° of GRS 1915+105 had free normalizations.

3.4. GX 339–4

There are hints that the large X-ray outburst of 2010 was accompanied by $TS \geq 9$ detections on 1-d and 10-d timescales in the gamma-rays (Fig. 11). This can be seen in the apparent clustering of $TS \geq 9$ bins within the ~ 400 day duration of the X-ray flare. However, the significances in these bins are low ($\lesssim 4.5\sigma$) and so the data do not provide conclusive evidence of gamma-ray activity by GX 339–4 on 1-d or 10-d timescales in the nearly 4 years since the launch of *Fermi*. The known orbital period of 1.8 d (Jonker & Nelemans 2004) is not detected in the 0.1-d light curve. We can also rule out a detection on timescales of years given its non-inclusion in the 1FGL and 2FGL catalogs. This is de-

spite the fact that the source has shown multiple state transitions during this time, including the brightest radio emission ever detected from this source during the hard state (Corbel et al. 2010a), and the ejection of material along a relativistic jet colliding with the interstellar medium (Corbel et al. 2010b). On 11 days (out of 1369) the TS was at the level of 9 or above (Table 5). The KS-test probability of 73% suggests that the low-significance detections are likely spurious (Fig. 12). Based on a likelihood analysis of the 4-year data set in which the spectral parameters of GX 339–4 and nearby sources (including those of the galactic and extragalactic diffuse background emission) were allowed to vary, we obtain a 3σ upper limit of $1.6 \times 10^{-8} \text{ ph cm}^{-2} \text{ s}^{-1}$ on the persistent 0.1–10-GeV flux from GX 339–4.

4. Discussion

4.1. Gamma-ray emission from Cygnus X-3

Our analysis of Cyg X-3 produced results that are consistent with previous reports and provided additional insight into this μ QSO. We confirm all but one of the previously-reported gamma-ray detections at similar flux levels and significances. The lone exception is the last reported gamma-ray detection by *AGILE* (Piano et al. 2011).

Five new transient emission events (lasting ~ 1 day) were detected outside of any previously-known gamma-ray active epochs. Two of the five events satisfy the X-ray conditions necessary for triggering gamma-ray emission as defined by Corbel et al. (2012). A third criterion relating to radio emission also exists: in past gamma-ray detections, the radio emission was either quenched just prior to the appearance of gamma-rays, or it showed minor flaring with flux densities of ~ 0.1 – 0.6 Jy at 15 GHz. We checked the radio emission at 15 GHz on these dates with the Large Array of the Arcminute Microkelvin Imager (The AMI Consortium; Zwart et al. 2008), and found that the radio emission was nearly quenched (flux density ~ 10 mJy) on MJD 55092. For the other 4 candidate gamma-ray detections, the radio flux density varied between 0.05 Jy and 0.15 Jy, i.e., at the low end of the level of minor flaring that has been seen in previous gamma-ray outbursts.

One observable difference between leptonic and hadronic processes is the cutoff energy in the gamma-ray range of the spectral energy distribution (SED). In IC processes, the electrons can lose energy very

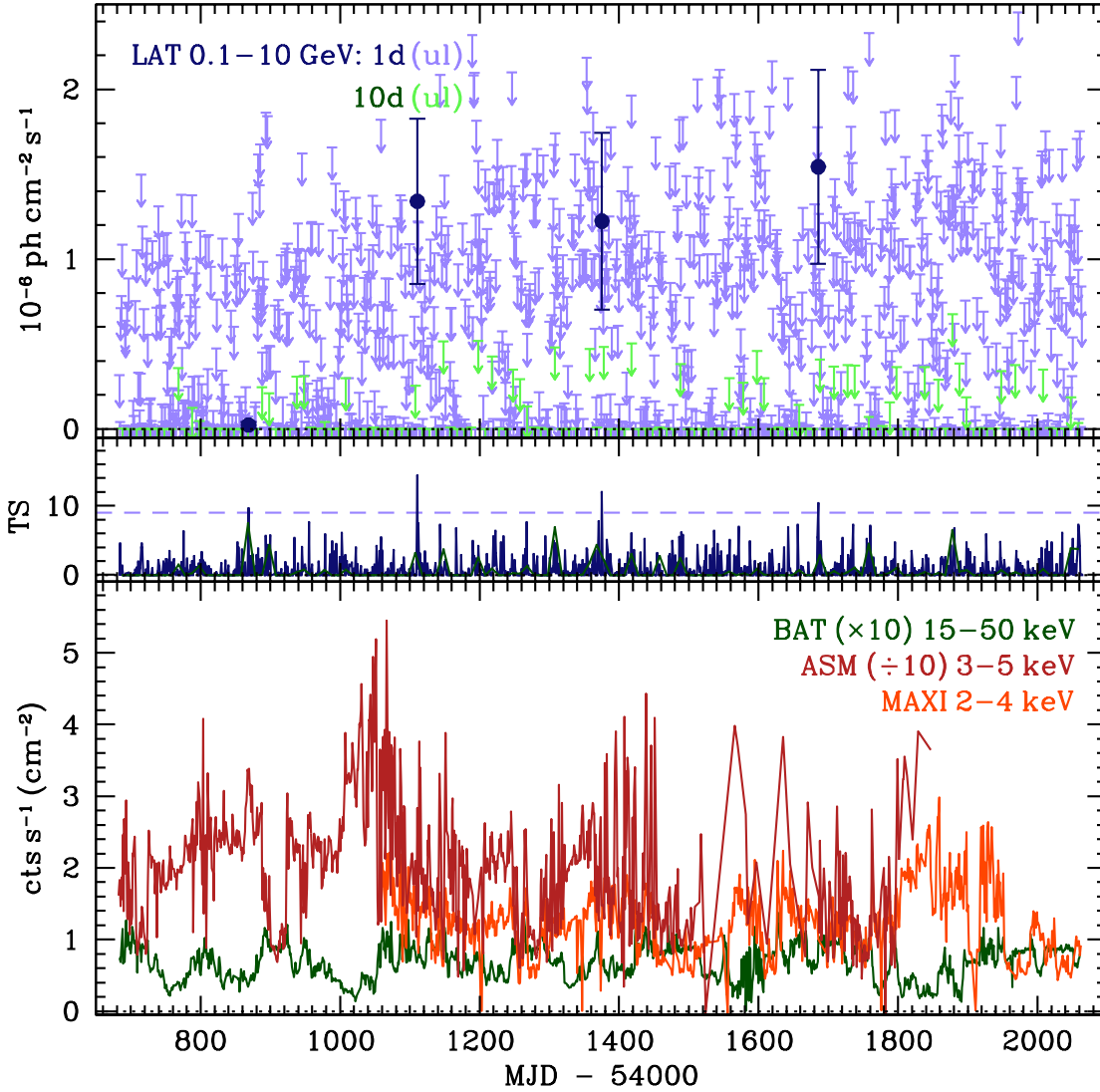


Fig. 9.— Same as Fig. 6 for GRS 1915+105.

rapidly by scattering and so they are unable to reach energies higher than a few TeV. Protons are not able to cool as efficiently and so the cutoff of the SED in the hadronic case extends to higher energies than in the leptonic case. The source flux and upper limits are not constraining enough to enable us to conclusively confirm or reject one of these scenarios.

Another observable difference between leptonic and hadronic processes is that neutrinos are the ex-

pected byproduct (besides gamma-rays) of the decay of neutral pions. Detecting neutrinos from Cyg X-3 would provide conclusive evidence that hadronic processes dominate the high-energy range of the SED (Christiansen et al. 2006; Baerwald & Guetta 2012). Observations gathered with IceCube (Karle et al. 2003) have not yielded a signature of a point-like neutrino source at the position of Cyg X-3, however, the expected neutrino flux is well below the current sen-

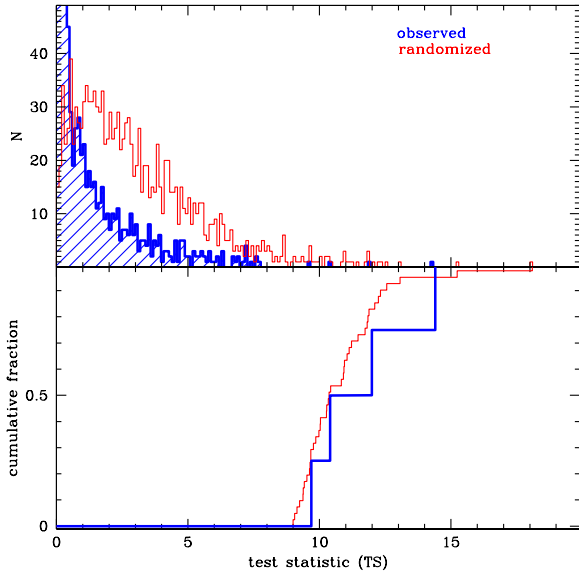


Fig. 10.— Same as Fig. 4 for GRS 1915+105. The KS-test probability is 83%.

sitivity limit of the instrument, and so more data are needed (Abbasi et al. 2011).

We detected significant ($\geq 5\sigma$ pre-trial correction) gamma-ray emission from Cyg X-3 on timescales of 10 days or more. Many of these 10-day-long bins overlap days on which transient outbursts were reported above ~ 100 MeV. These outbursts occasionally last a few days or weeks, so detecting emission in 10-d bins that are coincident with these epochs is not surprising. However, we did not anticipate finding a significant number of 10-d bins with high TS values outside of these gamma-active epochs, i.e., no more than would be expected from a likelihood analysis of a spurious unidentified gamma-ray source. Instead, we found that around half of the bins on the 10-d timescale had $TS \geq 20$ ($\geq 4.5\sigma$), and many of these were outside any known gamma-ray active epoch.

Contaminating emission from point-like or diffuse sources near Cyg X-3, which happens to reside in one of the most challenging regions of the sky for the LAT at these energies, could not be completely excluded. Neronov et al. (2012) found that the pulsar population contributes significant variability (on timescales of months) to the gamma-ray emission along the Galactic Plane. There is still a great deal of uncertainty in the spectral and spatial models of the sources in the

field, and this is especially true for the diffuse components. Nevertheless, these models represent the best fit available over the full data set. If we assume that the underlying emission is not from Cyg X-3 but due to the summed contribution of pulsars and other sources, this indicates that the normalizations of sources in the Cygnus region should be slightly higher (within the uncertainties) than they are currently set in the 2FGL catalog. This hypothesis can be rejected based on the fact that this emission is not present in the 10-d light curve of another object in this field with similar source spectral models: Cyg X-1.

If this is really coming from Cyg X-3, then it appears to be persistent gamma-ray emission. It might be that this system is unique given its extremely tight orbit and very massive donor star. The dense wind of the WR star being in such close proximity to an accreting CO can lead to shocks and particle acceleration inside turbulent accretion zones (Bednarek 2009). Fender et al. (2009) propose that steady, compact jets are expected from accreting black holes in the hard state. While Cyg X-3 was often observed to be in the hard state during the past 4 years, it is important to note that interactions between the accretion disk and the wind from the WR donor star lead to significant differences in the hard state spectrum of this source compared with the typical hard state of BH X-ray binaries (Szostek & Zdziarski 2008; Szostek et al. 2008). Another possibility is that the jet in Cyg X-3 never turns off, and that these jet electrons IC-scatter photons from the dense radiation field (Dermer & Böttcher 2006). If the plasma around the black hole is pair-dominated or mildly relativistic, then it can generate a gamma-ray “bump” at MeV energies, although not persistently (Liang & Dermer 1988; Dermer et al. 1996; Li et al. 1996; McConnell et al. 2000).

4.2. Possible confirmation of the gamma-ray detection of Cygnus X-1

In the absence of any indication that gamma-rays should be present from Cyg X-1 at a specific epoch, we would ascribe the few dozen low-significance detection days as being spurious. However, on three occasions (MJD 55118, MJD 55277, and MJD 55375), there was corroborating evidence from *AGILE* that gamma-rays were contemporaneously detected from this source. Our analysis of the LAT data supports the conclusions by the *AGILE* team that Cyg X-1 was gamma-ray active around these dates (Bulgarelli et al. 2010a; Sabatini et al. 2010b,a, 2013). Prior analysis of

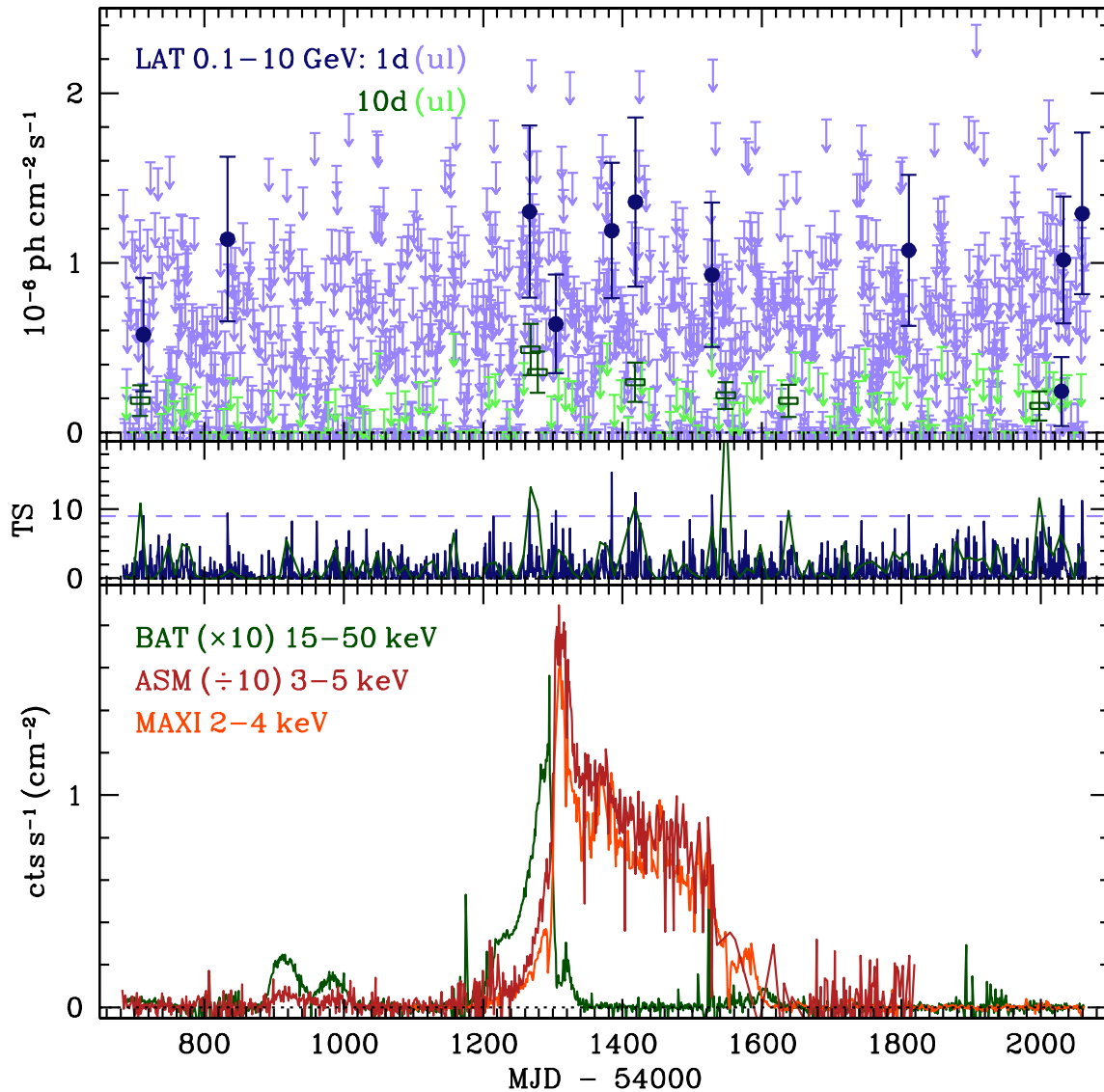


Fig. 11.— Same as Fig. 6 for GX 339-4.

the LAT data by our group, by others (e.g., Hill et al. 2011), and by the *AGILE* team (S. Sabatini: private communication) did not result in detections on these dates, and so the new Pass 7 data used in the current analysis is the first time that such excesses have been seen with the LAT.

In all three cases, the detection by *Fermi* preceded

that of *AGILE* by 1–2 days. Given the lower energy bandpass of *AGILE* compared with the LAT, this delay could be an indication that different parts of the jet are producing gamma-rays at different times. For example, gamma-rays produced near the base of the jet are first seen at high energies by *Fermi*, and 1–2 d later, these jet particles interact with the ISM producing lower-energy gamma-ray photons seen by *AGILE*.

Another possibility is that the delay is related to the cooling of accelerated jet particles via adiabatic expansion, or via synchrotron and brehmsstrahlung losses.

It has been proposed (and possibly observed once with *MAGIC*) that the production of gamma-rays should be maximized in IC and pair-production cascades near the phase of superior conjunction, i.e., when the massive donor star is between the observer and the CO, so that relativistic particles from the jet are beamed into the soft stellar radiation field (e.g. Bednarek 1997; Bednarek & Giovannelli 2007; Romero et al. 2010; Dubus et al. 2010). In Cyg X-1, the time of superior conjunction in MJD is $T_0 = 50077.995 + nP$ where n is the number of orbital cycles and P is the orbital period of 5.599829(16)d (Brocksopp et al. 1999).

The first LAT detection of Cyg X-1 contemporaneous with an *AGILE* detection was on MJD 55118. This integration window begins only 0.03 in phase after the nearest superior conjunction at MJD 55117.84(1) ($n = 900$). The second LAT detection contemporaneous with an *AGILE* detection (MJD 55277) is in the phase range 0.40–0.58 which overlaps inferior conjunction, while the *AGILE* integration window begins within 0.03 in phase of superior conjunction. The third LAT detection contemporaneous with an *AGILE* detection (MJD 55375) completely covers superior conjunction at MJD 55375.43(1) ($n = 946$). Keep in mind, however, that the short orbital period implies a $\sim 20\%$ probability that superior conjunction will occur on any given day. This is consistent with our observations whereby superior conjunction fell on 3 of the 21 days (15%) for which $TS \geq 9$.

On these 21 days with $TS \geq 9$, Cyg X-1 was around twice as likely (29% vs. 15%) to be in the transitional (or intermediate) state, where the conditions favor the formation and destruction of the relativistic jet. Both of the contemporaneous candidate gamma-ray detections by *AGILE* and *Fermi*-LAT were captured while the source was in the hard state, where a steady, low-velocity, compact jet is expected (Stirling et al. 2001). During the review of this article, Malyshev et al. (2013) reported a detection of Cyg X-1 with the LAT ($TS = 15.6$, $\sigma \sim 4$) by summing all available gamma-ray data during the hard state. The radio data from AMI shows Cyg X-1 at a flux density of 5–20 mJy at 15 GHz on these 2 days (and similar flux densities around the other 19 days) with no correlation between the level of radio emission and the significance of the candidate gamma-ray detections.

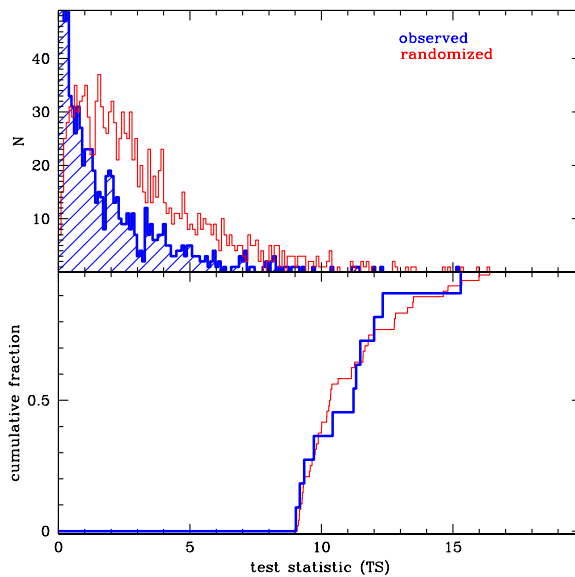


Fig. 12.— Same as Fig. 4 for GX 339–4. The KS-test probability is 73%.

The data do not allow us to paint a complete gamma-ray picture of Cyg X-1, but it is clearly a candidate gamma-ray binary that will continue to merit further observations and study in the high-energy domain.

4.3. Ingredients necessary to produce gamma-rays in μ QSOs

The recipe for producing transient gamma-rays in Cyg X-3 appears to be straightforward (Corbel et al. 2012): variable radio emission from the jet at the level of ~ 0.2 – 0.4 Jy (15 GHz); a soft X-ray flux in the ASM band above 3 cts s^{-1} (3–5 keV); and a hard X-ray flux in the BAT that transitions through 0.02 cts $s^{-1} cm^{-2}$ (15–50 keV). These LAT observations provide us with a more general list of ingredients necessary for gamma-ray production in μ QSOs.

According to leptonic and hadronic emission models, the jet is the primary ingredient necessary for producing gamma-rays in μ QSOs. These jets appear during specific X-ray emission states and so we have a direct relation between the soft vs. hard accretion-powered X-ray luminosity, accelerated particles and synchrotron emission from the jet, and the production of gamma-rays. Searches for gamma-rays from these

systems should focus on epochs with intense radio flaring. High-energy photons originating within the μ QSO can be photo-absorbed by the various radiation fields that are present (Aharonian 2004; Bosch-Ramon et al. 2008; Dubus et al. 2010). This absorption tends to dominate at energies $\gtrsim 10$ GeV, i.e., above the energy range considered in our analysis.

Only one μ QSO has been positively identified in the gamma-rays: Cyg X-3. There are possible (low-significance) detections of Cyg X-1 in the gamma-rays with MAGIC (Albert et al. 2007), with *AGILE* (Bulgarelli et al. 2010a; Sabatini et al. 2010b,a, 2013), and now with *Fermi*. Thus, the two μ QSOs with confirmed or possible gamma-ray detections are both HMXBs. In fact, all gamma-ray emitting binaries that have been detected thus far have a high-mass companion: this includes LS I+61°303, LS 5039, 1FGL J1018.6–5856 (Fermi LAT Collaboration et al. 2012), PSR B1259–63 (e.g., Tam et al. 2011), and possibly HESS J0632+057 (Hinton et al. 2009). There are no known gamma-ray emitting LMXBs including, as was shown here, GRS 1915+105 and GX 339–4.

This suggests that in addition to the radio jets, the nature of the donor star is an important ingredient in producing gamma-rays. High-mass stars feature a hot radiation field and dense winds which can serve: as soft seed photons necessary for pair creation and IC processes; and as a medium containing photons and protons with which the jet particles can interact. This ingredient is lacking in GRS 1915+105 and GX 339–4, which could explain why they were not detected in the gamma-rays despite the fact that both sources underwent major state transitions, including a huge radio outburst and relativistic ejection event from GX 339–4, during the 4-year monitoring period by the LAT. Thus, there are three possibilities for LMXB microquasars: 1) they do not emit any gamma-rays at all; 2) they emit some gamma-rays, but the flux is below the sensitivity limit of current telescopes; and 3) they emit gamma-rays, and the flux should be detectable. Scenarios 1 and 2 remain valid, but scenario 3 appears to be unlikely given our results (and those of other groups).

Leptonic and hadronic models predict orbital variations of the gamma-rays since the power of the collimated jet and the photon density of the soft radiation field will change along the orbit. As a result, the binary’s orbital configuration with respect to our line of sight strongly influences the observed gamma-ray spectrum from photon absorption or IC pro-

cesses (e.g. Bednarek 1997; Bednarek & Giovannelli 2007; Romero et al. 2010). For Cyg X-3, Abdo et al. (2009c) determined from the orbital modulations that its gamma-rays peak whenever the base of the jet is illuminated by the stellar UV photons with respect to our line of sight, i.e., near superior conjunction (Abdo et al. 2009c). For Cyg X-1, the possible MAGIC detection of TeV emission occurred near superior conjunction (i.e., with the CO behind the massive donor) when gamma-ray opacity is highest while the supergiant star provides a large target of UV seed photons (Albert et al. 2007; Romero et al. 2010). Superior conjunction fell within (or nearly within) the 1-d *Fermi* integration window on two of three occasions for which there were contemporaneous detections of Cyg X-1 by *Fermi*-LAT and *AGILE*.

High magnetic fields can suppress pair-creation cascades and lead to modulation of gamma-rays from IC scattering (e.g., Paredes 2008). Jet properties are not fully known for these systems, but their inclination with respect to the accretion disk, the observer, or the material at the termination shocks should influence the gamma-ray emission. For example, Cyg X-1 has a super-orbital period of ~ 300 d (e.g., Zdziarski et al. 2011) due to the precession of the accretion disk, although this variability timescale could not be detected in our gamma-ray data.

In summary, the ingredients that seem necessary for producing gamma-rays in μ QSOs are: 1) a radio jet; 2) dense winds and strong radiation fields typical of a high-mass donor star; and 3) an orbital configuration in which the CO is near superior conjunction. The magnetic field within the system and the jet inclination angle are also expected to play a role. The jet should be considered the primary ingredient in gamma-ray production, but our findings indicate, as others have suggested, that the nature of the donor star is also important. If the persistent emission that we detected from Cyg X-3 is confirmed, then this system, with its unique blend of extreme wind and orbital characteristics, may not even require a relativistic jet component to produce gamma-rays, although a compact jet could still be present.

5. Summary & Conclusions

In this work, we presented the results from a systematic search for gamma-ray emission from four μ QSOs using ~ 4 years of *Fermi*-LAT observations in the 0.1–10 GeV range. All four targets were very

active in the X-rays during this time so our gamma-ray monitoring sampled a variety of states and transitions.

Gamma-ray flares from Cyg X-3 were previously seen by *Fermi* and by *AGILE*, and our analysis reproduced all but one of these reported outbursts at similar fluxes and detection significances. Cyg X-3 was also detected at (pre-trial-corrected) significances of $\sim 5\sigma$ on five additional days not previously reported in the literature. The known outbursts, and the five new ones reported here, all coincided with epochs in which the soft and hard X-ray fluxes satisfied (or were close to satisfying) the criteria defined by Corbel et al. (2012), possibly satisfying the criteria on timescales less than the binning used here. Significant detections were seen for 10-d bins that overlap the known and new daily outbursts. In addition, there are numerous significant detections on 10-d timescales outside known gamma-ray flaring epochs. Its origin would therefore be unrelated to the relativistic jet, although a steady compact jet scenario is still a possibility, and would suggest that persistent gamma-ray emission from Cyg X-3 has been detected for the first time.

For the three other μ QSOs in our study, the situation is very different from that of Cyg X-3. There have been three reports of possible gamma-ray flares from Cyg X-1: one at TeV energies by MAGIC and three others in the MeV range by *AGILE*. Our analysis yielded 21 dozen low-significance detections on 1-d timescales from Cyg X-1, three of which were contemporaneous (within 1–2 days) with *AGILE* detections. However, we conclude that the other detections are probably spurious given the absence of compelling evidence of jet or gamma-ray activity. There are no previous reports of gamma-ray flaring by GRS 1915+105 and by GX 339–4 and our analysis did not uncover any significant detections of these sources on 1-d and 10-d timescales. This is despite the fact that both sources were very active in the past 4 years, with GX 339–4 emitting a large radio flare during our gamma-ray monitoring.

These results enable us to refine the list of ingredients that appear necessary for the detection of gamma-rays from microquasars. These ingredients are, in order of importance: the jet; the spectral type of the donor star (i.e., the dense, ionized winds of massive stars in HMXB systems are preferred); and the orientation of the jet with respect to the observer (i.e., the preferred orbital configuration of the system is superior conjunction). Other factors such as the magnetic field and the jet inclination angle could also affect the

emission of gamma-rays.

Even with the sensitivity of current instruments, detecting gamma-rays from μ QSOs is challenging due to the relative faintness of these systems and their location in the crowded regions of the Galactic Plane. Nevertheless, studying these objects in the gamma-rays, in tandem with multi-wavelength monitoring from the radio and X-rays, can provide valuable insights into the physics of jets and particle acceleration mechanisms.

The authors thank the anonymous referee whose constructive criticism led to an improved manuscript. AB thanks Stéphane Corbel, Robin H.D. Corbet, Victoria Grinberg, Michael McCullough, and Andrzej Zdziarski for useful discussions. AB and JAT acknowledge partial support from NASA Fermi Guest Observer Award NNX10AP83G. This research has made use of: data obtained from the High Energy Astrophysics Science Archive Research Center (HEASARC) provided by NASA’s Goddard Space Flight Center; the SIMBAD database operated at CDS, Strasbourg, France; NASA’s Astrophysics Data System Bibliographic Services; the Fermi Science Support Center; the Swift/BAT transient monitor results provided by the Swift/BAT team; and MAXI data provided by RIKEN, JAXA and the MAXI team.

REFERENCES

- Abbasi, R., et al. 2011, *ApJ*, 732, 18
- Abdo, A. A., et al. 2009a, *ApJ*, 701, L123
- . 2009b, *ApJ*, 706, L56
- . 2009c, *Science*, 326, 1512
- Aharonian, F., et al. 2005, *Science*, 309, 746
- Aharonian, F. A. 2004, *Very high energy cosmic gamma radiation : a crucial window on the extreme Universe* (River Edge, NJ: World Scientific Publishing)
- Albert, J., et al. 2006, *Science*, 312, 1771
- . 2007, *ApJ*, 665, L51
- Araudo, A. T., Bosch-Ramon, V., & Romero, G. E. 2009, *A&A*, 503, 673
- Atwood, W. B., et al. 2009, *ApJ*, 697, 1071
- Baerwald, P., & Guetta, D. 2012, *ArXiv e-prints*: 1212.1457

- Bednarek, W. 1997, *A&A*, 322, 523
- . 2009, *A&A*, 495, 919
- Bednarek, W., & Giovannelli, F. 2007, *A&A*, 464, 437
- Belloni, T., Homan, J., Casella, P., van der Klis, M., Nespoli, E., Lewin, W. H. G., Miller, J. M., & Méndez, M. 2005, *A&A*, 440, 207
- Belloni, T., Klein-Wolt, M., Méndez, M., van der Klis, M., & van Paradijs, J. 2000, *A&A*, 355, 271
- Blandford, R. D., & Znajek, R. L. 1977, *MNRAS*, 179, 433
- Böck, M., et al. 2011, *A&A*, 533, 8
- Bosch-Ramon, V., Khangulyan, D., & Aharonian, F. A. 2008, *A&A*, 489, L21
- Bosch-Ramon, V., Perucho, M., & Bordas, P. 2011, *A&A*, 528, 89
- Bosch-Ramon, V., Romero, G. E., & Paredes, J. M. 2006, *A&A*, 447, 263
- Bowyer, S., Byram, E. T., Chubb, T. A., & Friedman, H. 1965, *Science*, 147, 394
- Braes, L. L. E., & Miley, G. K. 1972, *Nature*, 237, 506
- Brocksopp, C., Tarasov, A. E., Lyuty, V. M., & Roche, P. 1999, *A&A*, 343, 861
- Bulgarelli, A., et al. 2010a, *ATel*, 2512
- . 2010b, *ATel*, 2609
- . 2011a, *ATel*, 3239
- . 2011b, *ATel*, 3141
- . 2011c, *ATel*, 3151
- . 2012, *A&A*, 538, A63
- Cadolle Bel, M., et al. 2006, *A&A*, 446, 591
- Castro-Tirado, A. J., Brandt, S., & Lund, N. 1992, *IAU Circ.*, 5590
- Christiansen, H. R., Orellana, M., & Romero, G. E. 2006, *Phys. Rev. D*, 73, 063012
- Corbel, S., Broderick, J., Brocksopp, C., Tzioumis, T., & ., R. F. 2010a, *ATel*, 2525
- Corbel, S., Fender, R. P., Tzioumis, A. K., Nowak, M., McIntyre, V., Durouchoux, P., & Sood, R. 2000, *A&A*, 359, 251
- Corbel, S., & Hays, E. 2010, *ATel*, 2646
- Corbel, S., Nowak, M. A., Fender, R. P., Tzioumis, A. K., & Markoff, S. 2003, *A&A*, 400, 1007
- Corbel, S., et al. 2010b, *ATel*, 2745
- . 2011, *ATel*, 3233
- . 2012, *MNRAS*, 421, 2947
- Corbet, R. H. D., et al. 2011, *ATel*, 3221
- Dermer, C. D., & Böttcher, M. 2006, *ApJ*, 643, 1081
- Dermer, C. D., Miller, J. A., & Li, H. 1996, *ApJ*, 456, 106
- Dubus, G. 2006, *A&A*, 451, 9
- Dubus, G., Cerutti, B., & Henri, G. 2010, *MNRAS*, 404, L55
- Fender, R. 2002, in *Lecture Notes in Physics*, Berlin Springer Verlag, Vol. 589, *Relativistic Flows in Astrophysics*, ed. A. W. Guthmann, M. Georganopoulos, A. Marcowith, & K. Manolakou, 101
- Fender, R., et al. 1999, *ApJ*, 519, L165
- Fender, R. P., Belloni, T. M., & Gallo, E. 2004, *MNRAS*, 355, 1105
- Fender, R. P., Homan, J., & Belloni, T. M. 2009, *MNRAS*, 396, 1370
- Fermi LAT Collaboration et al. 2012, *Science*, 335, 189
- Giacconi, R., Gorenstein, P., Gursky, H., & Waters, J. R. 1967, *ApJ*, 148, L119
- Gies, D. R., et al. 2008, *ApJ*, 678, 1237
- Grinberg, V., et al. 2013, *A&A*
- Hannikainen, D. C., et al. 2005, *A&A*, 435, 995
- Harlaftis, E. T., & Greiner, J. 2004, *A&A*, 414, L13
- Hill, A. B., Dubois, R., Torres, D. F., & Fermi LAT Collaboration. 2011, in *High-Energy Emission from Pulsars and their Systems*, ed. D. F. Torres & N. Rea, 498

- Hinton, J. A., et al. 2009, *ApJ*, 690, L101
- Hynes, R. I., Steeghs, D., Casares, J., Charles, P. A., & O'Brien, K. 2003, *ApJ*, 583, L95
- . 2004, *ApJ*, 609, 317
- Jonker, P. G., & Nelemans, G. 2004, *MNRAS*, 354, 355
- Karle, A., et al. 2003, *Nuclear Physics B Proceedings Supplements*, 118, 388
- Kaufman Bernadó, M. M., Romero, G. E., & Mirabel, I. F. 2002, *A&A*, 385, L10
- Klein-Wolt, M., Fender, R. P., Pooley, G. G., Belloni, T., Migliari, S., Morgan, E. H., & van der Klis, M. 2002, *MNRAS*, 331, 745
- Laurent, P., Rodriguez, J., Wilms, J., Cadolle Bel, M., Pottschmidt, K., & Grinberg, V. 2011, *Science*, 332, 438
- Li, H., Kusunose, M., & Liang, E. P. 1996, *A&AS*, 120, C167
- Liang, E. P., & Dermer, C. D. 1988, *ApJ*, 325, L39
- Ling, Z., Zhang, S. N., & Tang, S. 2009, *ApJ*, 695, 1111
- Lorenz, E. 2004, *New A Rev.*, 48, 339
- Malyshev, D., Zdziarski, A. A., & Chernyakova, M. 2013, *MNRAS*, in press, ArXiv e-prints: 1305.5920
- Markert, T. H., Canizares, C. R., Clark, G. W., Lewin, W. H. G., Schnopper, H. W., & Sprott, G. F. 1973, *ApJ*, 184, L67
- Mattox, J. R., et al. 1996, *ApJ*, 461, 396
- McClintock, J. E., & Remillard, R. A. 2006, *Black hole binaries* (Cambridge University Press, ed: Lewin, W. H. G. and van der Klis, M.), 157–213
- McConnell, M. L., et al. 2000, *ApJ*, 543, 928
- . 2002, *ApJ*, 572, 984
- Meier, D. L. 2001, *ApJ*, 548, L9
- Mirabel, I. F., & Rodríguez, L. F. 1994, *Nature*, 371, 46
- . 1999, *ARA&A*, 37, 409
- Negoro, H., et al. 2010, *ATel*, 2711
- Neronov, A., Malyshev, D., Chernyakova, M., & Lutovinov, A. 2012, *A&A*, 543, L9
- Owocki, S. P., Romero, G. E., Townsend, R. H. D., & Araudo, A. T. 2009, *ApJ*, 696, 690
- Paredes, J. M. 2008, in *American Institute of Physics Conference Series*, Vol. 1085, American Institute of Physics Conference Series, ed. F. A. Aharonian, W. Hofmann, & F. Rieger, 157–168
- Paredes, J. M. 2011a, ArXiv e-prints: 1101.4843
- . 2011b, *Mem. Soc. Astron. Italiana*, 82, 174
- Paredes, J. M., Martí, J., Ribó, M., & Massi, M. 2000, *Science*, 288, 2340
- Piano, G., et al. 2011, *ATel*, 3386
- . 2012, *A&A*, 545, 110
- Ray, P. S., et al. 2011, *ApJS*, 194, 17
- Reid, M. J., McClintock, J. E., Narayan, R., Gou, L., Remillard, R. A., & Orosz, J. A. 2011, *ApJ*, 742, 83
- Rodriguez, J., et al. 2008a, *ApJ*, 675, 1436
- . 2008b, *ApJ*, 675, 1449
- Romero, G. E., Del Valle, M. V., & Orellana, M. 2010, *A&A*, 518, 12
- Romero, G. E., Kaufman Bernadó, M. M., & Mirabel, I. F. 2002, *A&A*, 393, L61
- Romero, G. E., Torres, D. F., Kaufman Bernadó, M. M., & Mirabel, I. F. 2003, *A&A*, 410, L1
- Rushton, A., et al. 2010, *ATel*, 2714
- . 2012, *MNRAS*, 419, 3194
- Sabatini, S., et al. 2010a, *ATel*, 2715
- . 2010b, *ApJ*, 712, L10
- . 2013, *ApJ*, 766, 83
- Shrader, C. R., Titarchuk, L., & Shaposhnikov, N. 2010, *ApJ*, 718, 488
- Sitarek, J., & Bednarek, W. 2012, *MNRAS*, 421, 512

- Stirling, A. M., Spencer, R. E., de la Force, C. J., Garrett, M. A., Fender, R. P., & Ogle, R. N. 2001, *MNRAS*, 327, 1273
- Szostek, A., Dubus, G., Brun, F., de Naurois, M., & for the H. E. S. S. Collaboration. 2009, ArXiv e-prints: 0907.3034
- Szostek, A., & Zdziarski, A. A. 2008, *MNRAS*, 386, 593
- Szostek, A., Zdziarski, A. A., & McCollough, M. L. 2008, *MNRAS*, 388, 1001
- Tam, P. H. T., Huang, R. H. H., Takata, J., Hui, C. Y., Kong, A. K. H., & Cheng, K. S. 2011, *ApJ*, 736, L10
- Tavani, M., et al. 2009a, *Nature*, 462, 620
- . 2009b, *A&A*, 502, 995
- The AMI Consortium: Zwart, J. T. L., et al. 2008, *MNRAS*, 391, 1545
- The Fermi-LAT Collaboration. 2011, ArXiv e-prints: 1108.1435
- Tudose, V., et al. 2010, *ATel*, 2755
- van Kerkwijk, M. H., et al. 1992, *Nature*, 355, 703
- Vila, G. S., & Romero, G. E. 2010, *MNRAS*, 403, 1457
- Wen, L., Levine, A. M., Corbet, R. H. D., & Bradt, H. V. 2006, *ApJS*, 163, 372
- Williams, P. K. G., et al. 2011, *ApJ*, 733, L20
- Wilms, J., Nowak, M. A., Pottschmidt, K., Pooley, G. G., & Fritz, S. 2006, *A&A*, 447, 245
- Wilms, J., Pottschmidt, K., Pooley, G. G., Markoff, S., Nowak, M. A., Kreykenbohm, I., & Rothschild, R. E. 2007, *ApJ*, 663, L97
- Wilson-Hodge, C. A., & Case, G. 2010, *ATel*, 2721
- Zdziarski, A. A., Gierliński, M., Mikołajewska, J., Wardziński, G., Smith, D. M., Harmon, B. A., & Kitamoto, S. 2004, *MNRAS*, 351, 791
- Zdziarski, A. A., Maitra, C., Frankowski, A., Skinner, G. K., & Misra, R. 2012, *MNRAS*, 426, 1031
- Zdziarski, A. A., Mikołajewska, J., & Belczyński, K. 2013, *MNRAS*, 429, L104
- Zdziarski, A. A., Pooley, G. G., & Skinner, G. K. 2011, *MNRAS*, 412, 1985

TABLE 2
CANDIDATE DETECTIONS OF CYG X-3 BY *Fermi*-LAT

MJD	TS ^a	LAT ^b	ASM ^c	BAT ^d	criteria ^e	reported ^f
54708	21.7	1.8±0.5	1.298±0.161	0.048±0.002	N	new
54759	21.9	1.5±0.4	5.984±0.122	0.014±0.002	Y-	1
54768	27.0	1.9±0.5	6.050±0.107	0.028±0.003	Y+	1, 2
54804	21.3	1.7±0.4	6.207±0.187	0.002±0.001	Y-	1
54807	22.0	1.6±0.4	10.391±0.230	0.003±0.001	Y-	1
54809	33.7	1.8±0.4	8.334±0.258	0.005±0.001	Y-	1
54810	32.1	2.3±0.5	10.609±0.325	0.008±0.001	Y-	1
54811	21.9	1.6±0.5	9.835±0.300	0.009±0.002	Y-	1
54812	72.7	3.3±0.5	8.605±0.249	0.003±0.002	Y-	1, 2
54813	27.3	2.0±0.5	5.214±0.302	0.008±0.001	Y-	1
54814	40.1	2.2±0.4	7.491±0.249	0.022±0.002	Y+	1
54816	30.2	1.8±0.4	9.258±0.247	0.017±0.001	Y-	1
54911	23.1	1.6±0.4	2.114±0.143	0.028±0.003	Y+	new
54997	23.2	2.1±0.5	4.922±0.229	0.014±0.001	Y-	1, 3
55001	33.0	1.5±0.4	6.040±0.246	0.015±0.001	Y-	1, 3
55003	43.9	2.2±0.4	7.082±0.420	0.007±0.001	Y-	1, 2
55017	20.9	1.7±0.4	9.669±0.236	0.003±0.001	Y-	1
55021	23.1	1.3±0.4	10.768±0.276	0.006±0.001	Y-	1
55026	20.2	1.6±0.4	10.219±0.167	0.002±0.001	Y+	1, 2
55033	24.4	2.0±0.5	6.178±0.176	0.023±0.001	Y+	1
55034	58.2	3.3±0.5	8.639±0.244	0.013±0.001	Y-	1, 2
55035	52.2	2.7±0.5	9.664±0.234	0.011±0.001	Y-	1
55038	53.3	2.6±0.5	5.939±0.181	0.012±0.001	Y-	1
55041	20.5	1.5±0.5	5.560±0.238	0.022±0.001	Y+	1
55043	32.6	2.2±0.5	7.702±0.266	0.026±0.001	Y+	1
55092	23.8	1.7±0.4	6.789±0.200	0.018±0.003	Y-	new
55197	20.1	1.8±0.5	1.308±0.352	0.037±0.002	N	new
55339	22.0	2.0±0.5	7.874±0.560	0.008±0.001	Y-	4, 5
55341	27.6	2.2±0.5	5.830±0.308	0.010±0.002	Y-	5, 6
55586	22.1	1.4±0.4	5.219±0.548	0.021±0.001	Y+	7
55596	32.4	2.4±0.5	3.580±0.450	0.018±0.001	Y-	7
55600	30.1	2.6±0.6	8.650±0.850	0.018±0.001	Y-	7, 8
55607	31.5	2.0±0.5	6.220±1.420	0.011±0.002	Y-	7
55642	51.7	2.1±0.4	2.740±0.750	0.006±0.001	N	7, 9, 10
55643	27.6	1.9±0.5	2.740±0.750	0.018±0.001	N	7
55890	20.1	1.3±0.4	2.620±1.050	0.036±0.002	N	new

NOTE.—Days (MJD) on which the test statistic ≥ 20 ($\geq 4.5\sigma$) at the position of Cyg X-3 from a likelihood analysis of *Fermi*-LAT observations in 0.1–10 GeV.

^aTest statistic on this date from *Fermi*-LAT.

^bPhoton flux on this date from *Fermi*-LAT (10^{-6} ph cm $^{-2}$ s $^{-1}$).

^cCount rate near this date from *RXTE*-ASM (cts s $^{-1}$ in 3–5 keV).

^dCount rate near this date from *Swift*-BAT (cts s $^{-1}$ cm $^{-2}$ in 15–50 keV).

^eWhether the X-ray criteria as defined by Corbel et al. (2012) were satisfied: i.e., if on the listed date, Cyg X-3 had a count rate ≥ 3 cts s $^{-1}$ in the ASM band, and a count rate that passes the critical value of 0.02 cts s $^{-1}$ in the BAT band (“Y+” if the BAT rate has risen above 0.02, and “Y-” if the BAT rate has dropped below 0.02). The ASM data are degraded after MJD 55200 (e.g., Grinberg et al. 2013).

^fContemporaneous gamma-ray detections by *Fermi*-LAT or by *AGILE*: (1) Abdo et al. (2009c); (2) Piano et al. (2012); (3) Bulgarelli et al. (2012); (4) Bulgarelli et al. (2010b); (5) Corbel & Hays (2010); (6) Williams et al. (2011); (7) Corbel et al. (2012); (8) Bulgarelli et al. (2011c); (9) Corbel et al. (2011); (10) Bulgarelli et al. (2011a).

TABLE 3
CANDIDATE DETECTIONS OF CYG X-1 BY *Fermi*-LAT

MJD	TS ^a	LAT ^b	ASM ^c	BAT ^d	state ^e	reported ^f
54735	9.3	0.8±0.4	5.969±0.124	0.179±0.007	hard	
54923	13.1	~0.02	6.863±0.140	0.203±0.007	hard	
55001	9.7	~0.3	12.021±0.277	0.234±0.009	intermediate	
55057	12.5	0.3±0.2	6.082±0.319	0.184±0.007	hard	
55108	9.6	0.8±0.3	6.050±0.181	0.157±0.006	hard	
55118	13.1	0.9±0.4	6.109±0.149	0.166±0.006	hard	1
55137	11.9	1.1±0.4	6.397±0.242	0.179±0.007	hard	
55154	10.8	0.9±0.3	8.006±0.438	0.225±0.009	hard	
55160	10.3	0.8±0.3	7.478±0.257	0.180±0.007	intermediate	
55223	9.6	~0.2	6.813±0.239	0.284±0.014	hard	
55277	17.1	1.4±0.4	8.996±0.176	0.267±0.010	hard	2
55283	9.9	~0.1	6.145±0.199	0.187±0.007	hard	
55292	9.4	0.4±0.3	5.823±0.211	0.159±0.006	hard	
55361	9.8	~0.1	6.925±0.241	0.184±0.007	hard	
55375	10.2	~0.2	9.675±0.406	0.149±0.006	hard	3
55671	15.2	1.1±0.4	7.300±1.810	0.075±0.003	intermediate	
55738	12.4	0.5±0.3	2.275±0.491	0.109±0.004	hard	
55809	11.1	1.3±0.5	3.809±1.030	0.039±0.002	soft	
55913	12.4	0.3±0.2	—	0.150±0.005	intermediate	
55931	10.4	1.0±0.5	—	0.178±0.006	hard	
55941	12.5	1.0±0.3	—	0.146±0.005	intermediate	

NOTE.—Days (MJD) on which the test statistic ≥ 9 ($\geq 3\sigma$) at the position of Cyg X-1 from a likelihood analysis of *Fermi*-LAT observations in 0.1–10 GeV.

^aTest statistic on this date from *Fermi*-LAT.

^bPhoton flux on this date from *Fermi*-LAT (10^{-6} ph cm⁻² s⁻¹).

^cCount rate near this date from *RXTE*-ASM (cts s⁻¹ in 3–5 keV).

^dCount rate near this date from *Swift*-BAT (cts s⁻¹ cm⁻² in 15–50 keV).

^eX-ray state as defined by Grinberg et al. (2013).

^fContemporaneous gamma-ray detections by *AGILE*: (1) Sabatini et al. (2010b); (2) Bulgarelli et al. (2010a); (3) Sabatini et al. (2010a).

TABLE 4
CANDIDATE DETECTIONS OF GRS 1915+105 BY *Fermi*-LAT

MJD	TS ^a	LAT ^b	ASM ^c	BAT ^d
54868	9.7	0.023±0.017	33.070±0.300	0.034± 0.014
55110	14.4	1.340±0.487	28.393±0.506	0.068±0.003
55375	12.0	1.223±0.520	14.726±0.482	0.068±0.004
55685	10.4	1.543±0.572	15.965±0.970	0.070±0.003

NOTE.—Days (MJD) on which the test statistic ≥ 9 ($\geq 3\sigma$) at the position of GRS 1915+105 from a likelihood analysis of *Fermi*-LAT observations in 0.1–10 GeV.

^aTest statistic on this date from *Fermi*-LAT.

^bPhoton flux on this date from *Fermi*-LAT (10^{-6} ph cm⁻² s⁻¹).

^cCount rate near this date from *RXTE*-ASM (cts s⁻¹ in 3–5 keV).

^dCount rate near this date from *Swift*-BAT (cts s⁻¹ cm⁻² in 15–50 keV).

TABLE 5
CANDIDATE DETECTIONS OF GX 339–4 BY *Fermi*-LAT

MJD	TS ^a	LAT ^b	ASM ^c	BAT ^d
54712	9.0	0.576±0.333	−0.064±0.230	0.003±0.001
54833	9.3	1.139±0.485	−0.204±0.667	0.003±0.003
55266	11.5	1.301±0.507	2.076±0.260	0.061±0.002
55304	9.7	0.639±0.291	17.390±2.950	0.025±0.001
55384	15.3	1.190±0.399	9.665±0.496	0.001±0.001
55418	12.3	1.359±0.498	6.283±0.514	0.000±0.001
55528	12.0	0.929±0.426	0.470±1.000	0.018±0.007
55810	9.2	1.073±0.445	2.440±1.780	0.000±0.001
56029	11.3	0.242±0.203	—	0.001±0.001
56032	10.4	1.017±0.374	—	0.000±0.001
56059	11.2	1.291±0.477	—	0.000±0.001

NOTE.—Days (MJD) on which the test statistic ≥ 9 ($\geq 3\sigma$) at the position of GX 339–4 from a likelihood analysis of *Fermi*-LAT observations in 0.1–10 GeV.

^aTest statistic on this date from *Fermi*-LAT.

^bPhoton flux on this date from *Fermi*-LAT (10^{-6} ph cm $^{-2}$ s $^{-1}$).

^cCount rate near this date from *RXTE*-ASM (cts s $^{-1}$ in 3–5 keV).

^dCount rate near this date from *Swift*-BAT (cts s $^{-1}$ cm $^{-2}$ in 15–50 keV).